A multiscale analysis of the hotspot dynamics during the deceleration phase of inertial confinement capsules

Josselin Garnier[a)]
Laboratoire de Statistique et Probabilités, Université Paul Sabatier, 118 Route de Narbonne, 31062 Toulouse Cedex 4, France

Catherine Cherfils
Commissariat à l'Energie Atomique, Direction des Applications Militaires, Boîte Postale 12, 91680 Bruyères le Châtel, France

(Received 23 July 2004; accepted 5 October 2004; published online 14 December 2004)

This paper is devoted to the study of the deceleration phase of inertial confinement capsules. First the self-similar flow exhibited by Betti *et al.* [Phys. Plasmas **8**, 5257 (2001)] is proved to be an attractor in the sense that arbitrary initial conditions converge towards this solution. The convergence rate depends on the ablation process and heat conductivity and it is shown to be a power law of the increase rate of the hotspot mass. Second the thin layer that separates the hotspot from the cold shell is described and it is shown that it also converges to a locally self-similar profile. By using and generalizing a shell model introduced by Betti *et al.* [Phys. Plasmas **9**, 2277 (2002)] a closed system of ordinary differential equations for the main hydrodynamic variables is derived. Finally the linear growth rates of the deceleration phase Rayleigh–Taylor instabilities are computed taking into account ablation and spherical convergence. Significant differences are exhibited between directly and indirectly driven capsules. © *2005 American Institute of Physics*.
[DOI: 10.1063/1.1825389]

I. INTRODUCTION

The dynamics of the deceleration phase in inertial confinement fusion (ICF) experiments has recently been the subject of intense research.[1–6] In ICF a spherical capsule of cryogenic deuterium-tritium (DT) fuel and filled with gaseous DT is imploded by laser or x-ray irradiation.[7] The irradiation is designed to drive multiple shocks through the shell to minimize entropy. These shocks merge into a single one before reaching the center of the capsule, then this shock is reflected off the center. When interacting with the shell inner surface, the shock slows down the shell in an impulsive manner and generates a new shock that converges towards the center. A series of shocks are then reflected off the center and the shell inner surface increasing the pressure of the low-density gaseous hotspot enclosed by the shell. Eventually the gas inside the hotspot reaches a pressure large enough to slow down the shell in a continuous manner. The so-called deceleration phase then develops at the shell inner surface. Betti *et al.* have recently proposed an analysis of the hotspot dynamics where all hydrodynamic quantities are calculated by assuming a self-similar internal energy profile.[2] We shall revisit this work and prove in particular that any arbitrary initial condition at the beginning of the deceleration phase quickly converges to this self-similar solution. We shall prove a similar result at a microscopic level by showing that the thin layer can also be described in terms of an attractive self-similar small-scale profile which matches the macroscopic profiles inside the hotspot and inside the shell. The description of the thin layer provides all relevant parameters necessary for the study of the Rayleigh–Taylor (RT) growth rates.

It is well known that RT instabilities are a limiting factor in ICF experiments. The RT instability occurs when a fluid accelerates another fluid of higher density. This happens in ICF targets at the outer shell surface during the acceleration phase and at the shell inner surface during the deceleration phase. This phenomenon may dramatically reduce the performance of ICF experiments by degrading the symmetry of implosion[7] or even by breaking the shell. In ICF targets the ablation process and the thermal transport play a central role.[8] It has been shown by several authors that the ablative RT instability growth is stabilized relative to classical RT during the acceleration phase at the outer shell surface.[9,10] In this paper the growth rates of RT instabilities at the shell inner surface are studied during the deceleration phase with a model that takes into account ablation, finite-density-gradient scale length, heat conduction, and spherical convergence.

The paper is organized as follows. In Sec. II we write the equations of motion in spherical geometry. Section III is devoted to the description of the attractive self-similar solution. We study carefully the thin layer at the edge of the hotspot in Sec. IV. We close the system by introducing and discussing different shell models in Sec. V. Finally we compute the RT growth rates of the shell inner surface in Sec. VI.

II. THE MODEL IN SPHERICAL GEOMETRY

The model is based on the mass, momentum, and energy equations

$$\partial_t(\rho) + \nabla \cdot (\rho \mathbf{u}) = 0, \tag{1}$$

a)Electronic mail: garnier@cict.fr; URL:http://www.lsp.ups-tlse.fr/Garnier

$$\partial_t(\rho\mathbf{u}) + \boldsymbol{\nabla}\cdot(\rho\mathbf{u}\otimes\mathbf{u}) + \nabla p = 0, \tag{2}$$

$$\partial_t(p) + \boldsymbol{\nabla}\cdot[\gamma p\mathbf{u} - (\gamma-1)\kappa(T)\nabla T] = S, \tag{3}$$

where $S=(\gamma-1)\rho^2 E_\alpha\langle\sigma v\rangle/(4m_i^2)$ is the source term given by nuclear reaction, E_α is the α-particle energy, $\langle\sigma v\rangle$ is the fusion reaction rate, and m_i is the ion mass. $\kappa(T)=\chi T^\nu$ is the Spitzer thermal conductivity. This system is completed by the standard ideal gas equation of state (EOS) $p=(\gamma-1)c_v\rho T$ with $\gamma=5/3$ for a monoatomic gas. c_v is the specific heat at constant volume. We approximate the fusion cross section by a quadratic form $\langle\sigma v\rangle\simeq S_\alpha T^2$. Such an approximation is valid as long as $6<T<20$ keV which is the range relevant to ignition in ICF.[2] For subsonic flows we can expand the solution to the equations of motion by a formal expansion in powers of the Mach number. To lowest order we get the flat pressure approximation $p(t,\mathbf{r})=p(t)$. To order one the mass and energy equations read in spherical geometry as

$$\frac{\partial\rho}{\partial t} + \frac{1}{r^2}\frac{\partial}{\partial r}(r^2\rho u) = 0, \tag{4}$$

$$\frac{\partial p}{\partial t} + \frac{\gamma p}{r^2}\frac{\partial}{\partial r}(r^2u) - \frac{\overline{\chi}}{r^2}\frac{\partial}{\partial r}\left(r^2T^\nu\frac{\partial}{\partial r}(T)\right) = \mu_\alpha p^2, \tag{5}$$

where $\overline{\chi}=(\gamma-1)\chi$ and $\mu_\alpha=E_\alpha S_\alpha/[4(\gamma-1)m_i^2c_v^2]$. The momentum equation describes the fluctuations of the pressure and it can be integrated *a posteriori*. The energy equation can be integrated to obtain the expression of the velocity flow

$$u(r,t) = \frac{\overline{\chi}T^\nu}{\gamma p}\frac{\partial T}{\partial r} + \frac{r}{3\gamma}\left(\mu_\alpha p - \frac{p'}{p}\right). \tag{6}$$

Substituting into the mass equation and eliminating the density by the EOS, we get the equation governing the evolution of the temperature

$$\left(p'\frac{\gamma-1}{\gamma} + \frac{\mu_\alpha}{\gamma}p^2\right)T - p\frac{\partial T}{\partial t} - \frac{r}{3\gamma}(\mu_\alpha p^2 - p')\frac{\partial T}{\partial r} + \frac{\overline{\chi}T^2}{\gamma r^2}\frac{\partial}{\partial r}\left(r^2T^{\nu-1}\frac{\partial T}{\partial r}\right) = 0. \tag{7}$$

The initial conditions in ICF are such that the temperature in the shell T_∞ is much less than the central hotspot temperature T_c. Denoting by δ this small ratio, the temperature is of order T_c inside a sphere with radius $R_h(t)$ (delimiting the so-called hotspot), and of order δT_c outside the sphere. We shall see in Sec. IV that the hotspot is actually surrounded by a thin layer with thickness $\delta^\nu R_h$ where the temperature and the heat flow undergo a rapid transition between the two regimes. By Eq. (6) the velocity at the edge of the hotspot satisfies

$$(p' - \mu_\alpha p^2)\frac{R_h^3}{3} + \gamma p R_h^2 u[R_h(t),t] = \overline{\chi}R_h^2T^\nu\partial_r T. \tag{8}$$

The right-hand member is 0 to lowest order in δ because the heat flux is small at the edge of the hotspot. The velocity at R_h is the sum of the surface motion and the ablative flow $u[R_h(t),t]=R_h'(t)+V_{loc}(t)$. The local ablation velocity is much smaller than the interface velocity (we shall study precisely the local behavior at the interface in Sec. IV and show that V_{loc} is of the order of $\delta R_h'$). To lowest order (8) can thus be simplified into

$$\frac{p' - \mu_\alpha p^2}{p} = -3\gamma\frac{R_h'}{R_h}. \tag{9}$$

III. SELF-SIMILAR DYNAMICS

In this section we revisit the derivation of a self-similar solution that was first obtained in Ref. 2. Let us seek a self-similar form for the temperature profile

$$T(t,r) = T_c(t)F_T\left(\frac{r}{R_h(t)}\right), \tag{10}$$

with $F_T(0)=1$. In the near-isobaric framework, the density profile is then also self-similar $\rho(t,r)=\rho_c(t)/F_T[r/R_h(t)]$. $T_c(t)$ [resp. $\rho_c(t)$] is the central hotspot temperature [resp. density]. Substituting the ansatz (10) into Eq. (7) and using the identity (9), we get the compatibility equation

$$[x(F_T'F_T^{\nu-1})'(x) + 2F_T'F_T^{\nu-1}(x)]\left[\frac{\overline{\chi}T_c^{\nu+2}}{\gamma R_h^2(t)}\right] + [xF_T^{-1}(x)] \times\left[\left(p'\frac{\gamma-1}{\gamma} + \frac{\mu_\alpha}{\gamma}p^2\right)T_c - pT_c'\right] = 0, \tag{11}$$

which involves the two independent variables t and $x=r/R_h(t)$. The EOS implies $\rho_c'/\rho_c+T_c'/T_c=p'/p$. The mass of the hotspot M_h satisfies $3R_h'/R_h+\rho_c'/\rho_c=M_h'/M_h$. Using once again Eq. (9), the expression in the last brackets in Eq. (11) can be rewritten as $[p'(\gamma-1)/\gamma+(\mu_\alpha/\gamma)p^2]T_c-pT_c' = T_cpM_h'/M_h$. As a result the compatibility equation admits a solution if the mass of the hotspot satisfies the differential equation

$$\frac{M_h'(t)}{M_h(t)} = A_\nu\frac{\overline{\chi}T_c^{\nu+1}(t)}{\gamma R_h^2(t)p(t)} \tag{12}$$

for a constant A_ν that also parameterizes the equation that F_T must satisfy

$$x(F_T'F_T^{\nu-1})'(x) + 2F_T'F_T^{\nu-1}(x) + A_\nu xF_T^{-1}(x) = 0. \tag{13}$$

By defining $G(x)=F_T^\nu(x)$ this equation can be rewritten in the following simple form:

$$xG''(x) + 2G'(x) + \nu A_\nu xG^{-1/\nu}(x) = 0. \tag{14}$$

The profile G must satisfy $G(0)=1$, $G'(0)=0$, and the temperature becomes evanescent at the edge of the hotspot $x=1$ so that $G(1)=0$. These conditions are fulfilled only for a particular value of A_ν that can be determined as follows. We consider G_1 the solution $xG_1''+2G_1'+xG_1^{-1/\nu}=0$ starting from $G_1(0)=1$, $G_1'(0)=0$. We establish numerically that the first zero of G_1 is at $x_\nu\simeq 2.253$ for $\nu=5/2$. The profile G can then be expressed in terms of G_1 as $G(x)=G_1(xx_\nu)$. Thus $A_\nu=x_\nu^2/\nu\simeq 2.03$ for $\nu=5/2$. The function G is plotted in the left plot of Fig. 1 for $\nu=5/2$. We can also give the value of the hotspot mass $M_h(t)=m_\nu\rho_c(t)R_h(t)^3$ where $m_\nu=4\pi\int_0^1 x^2/F_T(x)dx$ which is equal to $m_\nu\simeq 7.33$ for $\nu=5/2$.

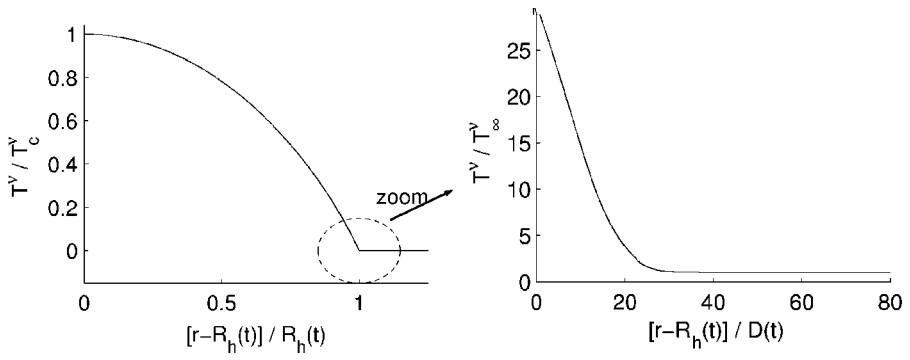

FIG. 1. Heat conductivity profile $T(t,r)^\nu$ for $\nu=5/2$. At the macroscopic level (left picture) the profile is described by the function $T_c^\nu(t)G[r/R_h(t)]$, where $T_c(t)$ is the central temperature and G is the normalized profile obtained from the self-similar analysis of Sec. III. Close to the edge of the hotspot the function G decays linearly $G(x)\simeq C_\nu(1-x)$, $0<1-x\ll 1$ with $C_\nu\simeq 2.96$. At the microscopic level around $r=R_h$ (right picture) the profile is described by the function $T_\infty^\nu(t)g\{[r-R_h(t)]/D(t)\}$ where $T_\infty(t)$ is the temperature in the inner region of the shell, the width $D(t)$ is given by (25), and the normalized profile g is obtained from the thin layer analysis of Sec. IV. This microscopic profile matches the self-similar high-temperature profile in the hotspot and the low temperature in the shell.

To sum up, if the initial temperature profile is of the form $T(t=0,r)=T_{c0}F_T[r/R_h(0)]$ with $F_T=G^{1/\nu}$, then the dynamics is self-similar and described by Eq. (10). The hotspot radius is obtained by integration of Eq. (9)

$$R_h(t)=R_h(0)\left(\frac{p(t)}{p(0)}\right)^{-1/(3\gamma)}\exp\left(\frac{\mu_\alpha}{3\gamma}\int_0^t p(s)ds\right).$$

The mass of the hotspot can then be integrated

$$M_h(t)=\left[M_h(0)^{\nu+1}+c_1c_v^{-\nu-1}\overline{\chi}[R_h(0)^3\gamma p(0)]^{(3\nu+1)/(3\gamma)}\right.$$
$$\times\int_0^t p(s)^{[3(\gamma-1)\nu-1]/(3\gamma)}$$
$$\left.\times\exp\left(\frac{(3\nu+1)\mu_\alpha}{3\gamma}\int_0^s p(\tau)d\tau\right)ds\right]^{1/(\nu+1)},$$

with $c_1=[(\nu+1)A_\nu m_\nu^{\nu+1}]/[\gamma(\gamma-1)^{\nu+1}]\simeq 1.88\times 10^4$ for $\nu=5/2$ and $\gamma=5/3$. The temperature profile is Eq. (10) with the central hotspot temperature given by

$$T_c(t)=T_c(0)\frac{M_h(0)p(0)^{1/\gamma}}{M_h(t)p(t)^{1/\gamma}}\exp\left(\frac{\mu_\alpha}{\gamma}\int_0^t p(s)ds\right).$$

Substituting into Eq. (6) establishes the velocity profile

$$u(t,r)=R_h'(t)\left[\frac{r}{R_h(t)}-\epsilon(t)F_T^\nu F_T'\left(\frac{r}{R_h(t)}\right)\right], \tag{15}$$

with $\epsilon(t)=A_\nu^{-1}[M_h'/M_h(t)]/[|R_h'|/R_h(t)]$. In typical ICF configurations ϵ is increasing with time. To sum up, all hydrodynamic quantities can be computed in terms of the hotspot pressure $p(t)$. We shall address in Sec. V different shell models. The coupling between the hotspot and the shell provides additional equations that close the system. However, an interesting issue that was not addressed in Refs. 2 and 3 is whether the self-similar profile will be actually observed in an ICF experiment. The end of the section is devoted to this issue.

Let us consider an arbitrary initial condition with temperature profile $T(t=0,r)$ which is compactly supported in a sphere whose radius is denoted by $R_h(0)$. The initial pressure and mass in this sphere are denoted by $p(0)$ and $M_h(0)$, respectively. We write $T(t=0,r)=T_0(t=0,r)+T_1(t=0,r)$ where T_0 is the self-similar profile that corresponds to the mass $M_h(0)$ and radius $R_h(0)$, that is to say

$$T_0(t=0,r)=F_T\left(\frac{r}{R_h(0)}\right)\frac{m_\nu R_h(0)^3p(0)}{c_v(\gamma-1)M_h(0)}.$$

If $T_1(t=0,r)$ is zero, then the flow is self-similar and obeys the dynamics described in Sec. III. If $T_1(t=0,r)$ is nonzero but small enough, then we can linearize the solution near the self-similar flow $T(t,r)=T_0(t,r)+T_1(t,r)$. By integrating the linearized EOS and energy conservation we can express the perturbed density and velocity in terms of the perturbed temperature

$$\rho_1(t,r)=-\frac{p(t)}{c_v(\gamma-1)T_0^2(t,r)}T_1(t,r), \tag{16}$$

$$u_1(t,r)=\frac{\vec{\chi}}{\gamma p(t)}\frac{\partial}{\partial r}[T_0^\nu T_1(t,r)]. \tag{17}$$

We introduce $\xi(t,r)=T_1(t,r)/T_0^2(t,r)$ which satisfies the equation

$$\left(\frac{p'}{p}+3\frac{R_h'}{R_h}\right)\xi+\frac{\partial\xi}{\partial t}+\frac{R_h'}{R_h}r\frac{\partial\xi}{\partial r}-\frac{\overline{\chi}}{\gamma pr^2}\frac{\partial}{\partial r}\left(r^2\frac{\partial T_0^{\nu+1}\xi}{\partial r}\right)=0. \tag{18}$$

ξ can be written in the form

$$\xi(t,r)=\frac{1}{R_h^2p(t)r}F_T^{-\nu-1}\left(\frac{r}{R_h(t)}\right)\breve{\xi}\left(\frac{r}{R_h(t)},\tau(t)\right). \tag{19}$$

The function $\tau(t)$ characterizes the time flow in terms of the ablation process

$$\tau(t)=\frac{1}{A_\nu}\ln\left(\frac{M_h(t)}{M_h(0)}\right). \tag{20}$$

At $r=0$, $\xi(\tau,0)$ takes some finite value, so that $\check{\xi}(\tau,0)=0$ at $x=0$. For $r\geqslant R_g$, the diffusive part in Eq. (18) vanishes and only the transport term remains. As a result, for $x\geqslant 1$, the equation satisfied by $\check{\xi}$ is simply $\partial_\tau\check{\xi}=0$, which shows that $\check{\xi}(\tau,1)=\check{\xi}(0,1)=0$. Finally, for $x\in(0,1)$, $\check{\xi}$ is solution of the one-dimensional diffusion equation

$$\partial_\tau\check{\xi}=F_T^{\nu+1}(x)\partial_x^2\check{\xi}, \tag{21}$$

with the boundary conditions $\check{\xi}(\tau,0)=\check{\xi}(\tau,1)=0$.

By differentiating $\int_0^{R_h(t)}\rho_1(r,t)r^2dr$ we get that the perturbation of the density ρ_1 does not modify the evolution of the mass $M_h(t)$, in the sense that

$$M_h(t)=4\pi\int_0^{R_h(t)}\rho_0(r,t)r^2dr.$$

The section is devoted to the study of the difference T_1 between the solution T of the real system and the self-similar solution T_0. We are going to prove two quantitative estimates that give the convergence rate of the solution towards the self-similar solution. These two results give two different estimates for two different weighted quadratic norms of T_1.

Proposition. The convergence rate of the solution towards the self-similar solution is a power law in $M_h(0)/M_h(t)$. The following inequality holds true:

$$\frac{\displaystyle\int_0^{R_h(t)}(T_1^2/T_0^2)(t,r)\mu_t(r)r^2dr}{\displaystyle\int_0^{R_h(t)}\mu_t(r)r^2dr} \leqslant\left(\frac{M_h(0)}{M_h(t)}\right)^{2c_\nu}\frac{\displaystyle\int_0^{R_h(0)}(T_1^2/T_0^2)(0,r)\mu_0(r)r^2dr}{\displaystyle\int_0^{R_h(0)}\mu_0(r)r^2dr} \tag{22}$$

for $(\mu,c_\nu)=(\mu^{(a)},c_\nu^{(a)})$ or $=(\mu^{(b)},c_\nu^{(b)})$ where (a) $c_\nu^{(a)}\simeq 2.48$ for $\nu=5/2$, $\mu_t^{(a)}(r)=F_T^{(\nu-1)/2}[r/R_h(t)]$, (b) $c_\nu^{(b)}\simeq 3.51$ for $\nu=5/2$, $\mu_t^{(b)}(r)=F_T^{3(\nu-1)/2}[r/R_h(t)]$.

The Appendix is devoted to the mathematical proof of the proposition. This proposition demonstrates that the ablation process makes the flow converge to the self-similar solution. Thermal conduction is also important as it imposes the value of the power c_ν.

IV. ANALYSIS OF THE THIN LAYER

The preceding section was devoted to the macroscopic description of the hotspot. The analysis is carried out in the asymptotic framework where the temperature in the shell is much smaller than the central hotspot temperature. We have found that the temperature vanishes at the edge of the hotspot because the asymptotic analysis only takes into account leading order terms. We would like to study more carefully the thin layer that separates the hotspot from the cold shell. We accordingly impose the nonzero boundary condition

$$T(t,r)\xrightarrow{r\to\infty}T_\infty(t) \tag{23}$$

and we introduce $\delta=T_\infty(0)/T_c(0)$. We shall study the thin layer in the asymptotic framework $\delta\ll 1$. The temperature T_∞ could be considered as constant, but we shall address the general case where $T_\infty(t)$ is a slowly time-varying quantity which takes values with the same order of magnitude as $T_\infty(0)$. We accordingly introduce the normalized temperature $\hat{T}_\infty(t)=T_\infty(t)/T_\infty(0)$ and assume that $\hat{T}_\infty(t)=0(1)$. The central temperature is also a time-varying quantity, so we normalize it by introducing $\hat{T}_c(t)=T_c(t)/T_c(0)$ and by assuming $\hat{T}_c(t)=0(1)$. To study the thin layer we focus our attention to the vicinity of the edge and set

$$T(t,r)=T_\infty(t)f\left(\frac{r-R_h(t)}{D(t)}\right). \tag{24}$$

We aim at identifying the thickness $D(t)$ and the profile $f(x)$ of the local temperature profile. We also wish to prove that the temperature profile takes the form (24) locally. On the one hand, from the boundary condition (23) the profile f must satisfy $f(x)\to 1$ as $x\to+\infty$. On the other hand f should match the macroscopic self-similar temperature profile as $x\to-\infty$. For $0<1-r/R_h(t)\ll 1$ the macroscopic profile is of the form $T_c(t)C_\nu^{1/\nu}[1-r/R_h(t)]^{1/\nu}$ where $C_\nu=-G'(1^-)\simeq 2.96$ for $\nu=5/2$ (see Fig. 1). Thus $\delta\hat{T}_\infty(t)f(x)\simeq C_\nu^{1/\nu}|x|^{1/\nu}\hat{T}_c(t)\times[D(t)/R_h(t)]^{1/\nu}$ as $x\to-\infty$. This in turn imposes that the thickness of the layer is of order δ^ν and given by

$$D(t)=\delta^\nu\frac{R_h(t)}{\nu}\left(\frac{\hat{T}_\infty(t)}{\hat{T}_c(t)}\right)^\nu=\frac{R_h(t)}{\nu}\left(\frac{T_\infty(t)}{T_c(t)}\right)^\nu. \tag{25}$$

Furthermore the profile f must satisfy $f(x)\simeq|x|^{1/\nu}$ as $x\to-\infty$. By substituting Eq. (24) into Eq. (7) we get

$$\left[p'\frac{\gamma-1}{\gamma}+\frac{\mu_\alpha}{\gamma}p^2-p\frac{\hat{T}_\infty'}{\hat{T}_\infty}\right](t)f(x)+\left\{\frac{R_hp}{D}\left[\frac{R_h'}{R_h}+\frac{1}{3\gamma}\times\left(\frac{p'}{p}-\mu_\alpha p\right)\right](t)+x\left(\frac{D'p}{D}+\frac{p'-\mu_\alpha p^2}{3\gamma}\right)(t)\right\}f'(x) +\frac{\hat{\chi}\delta^{\nu+1}\hat{T}_\infty^{\nu+1}(t)}{\gamma}\left[\frac{f^{\nu+1}f'(x)}{DR_h(t)}+\frac{(\nu-1)f'^2f^\nu(x)+f^{\nu+1}f''(x)}{D(t)^2}\right]=0, \tag{26}$$

where $\hat{\chi}=\overline{\chi}T_c^{\nu+1}(0)$. The identity (9) cannot be applied directly because it is valid only at lowest order in δ. Here the correction in δ plays a role. We substitute $u(R_h(t),t)=R_h'(t)+V_{loc}(t)$ with $V_{loc}(t)=\delta\hat{V}_{loc}(t)$ into Eq. (8). Taking into account Eq. (25) we get

$$\frac{R_h'}{R_h}(t)+\frac{1}{3\gamma}\left(\frac{p'}{p}-\mu_\alpha p\right)(t)=\delta\left(-\hat{V}_{loc}(t)R_h(t)+\frac{C_\nu\hat{\chi}\hat{T}_c(t)^\nu\hat{T}_\infty(t)}{\gamma pR_h^2(t)}f^\nu(0)f'(0)\right).$$

Note that another scaling for $V_{loc}(t)$ would lead to a compatibility condition that has no solution. Substituting into Eq. (26) and collecting the terms with lowest order in δ, we get the effective compatibility equation

$$\left[-p\hat{V}_{loc}(t)+\frac{C_\nu\hat{\chi}\hat{T}_c^\nu(t)\hat{T}_\infty(t)}{\gamma R_h(t)}f^\nu(0)f'(0)\right]f'(x)$$
$$+\frac{C_\nu\hat{\chi}\hat{T}_c^\nu(t)\hat{T}_\infty(t)}{\gamma R_h(t)}[(\nu-1)f'^2f^\nu+f^{\nu+1}f''](x)=0.$$

Note that this compatibility equation holds true only if $\nu>1$. It is satisfied if the local velocity is of the form

$$\hat{V}_{loc}(t)=\frac{C_\nu\hat{\chi}\hat{T}_c^\nu(t)\hat{T}_\infty(t)}{\gamma pR_h(t)}[f^\nu(0)f'(0)-B_\nu], \tag{27}$$

where B_ν is a constant that also parameterizes the differential equation that f must satisfy

$$(\nu-1)f'^2f^\nu(x)+f^{\nu+1}f''(x)+B_\nu f'(x)=0. \tag{28}$$

By defining $g=f^\nu$ we can write this equation in the simple form $g''+B_\nu g'g^{-(\nu+1)/\nu}=0$. The boundary conditions in terms of g read $g(x)\to 1$ as $x\to+\infty$ and $g(x)\simeq|x|$ as $x\to-\infty$. Using the boundary condition at $+\infty$ the equation governing g can be integrated as

$$g'(x)=\nu B_\nu[g(x)^{-1/\nu}-1]. \tag{29}$$

The boundary condition at $-\infty$ thus imposes $B_\nu=1/\nu$. The function g is plotted in Fig. 1 for $\nu=5/2$. By substituting into Eq. (27) we obtain the local velocity

$$V_{loc}(t)=-\frac{C_\nu\overline{\chi}T_c(t)^\nu}{\nu\gamma pR_h(t)}T_\infty(t)f(0).$$

Note that $T_\infty(t)f(0)$ is the exact temperature at the edge $r=R_h(t)$ while the density at this point is $\rho_{loc}(t)=T_c(t)\rho_c(t)/[T_\infty(t)f(0)]$. The mass flow at the edge of the hotspot is accordingly

$$\rho_{loc}(t)V_{loc}(t)=-\frac{C_\nu\overline{\chi}T_c(t)^{\nu+1}\rho_c(t)}{\nu\gamma R_h(t)p(t)},$$

which is independent of the precise definition of the position of the edge, i.e., the mass flow is locally constant. We also get the variation of the mass of the hotspot

$$M_h'(t)=-4\pi R_h^2(t)\rho_{loc}(t)V_{loc}(t)$$
$$=\frac{4\pi C_\nu}{\nu}\frac{\overline{\chi}T_c(t)^{\nu+1}\rho_c(t)R_h(t)}{\gamma p(t)}. \tag{30}$$

The identity proved in the following lemma shows that Eq. (30) is the same as Eq. (12). In other words the compatibility equations for the macroscopic self-similar profile and for the microscopic local profile are identical. They are satisfied simultaneously. As we have shown that the self-similar profile is attractive, this property also holds true for the local profile.

Lemma. $A_\nu m_\nu=4\pi C_\nu/\nu\simeq 14.88$ for $\nu=5/2$.

Proof. m_ν is given by $m_\nu=\int_0^1 x^2G^{-1/\nu}(x)dx$. Using Eq. (14) satisfied by G, and integrating by part yields

$$m_\nu=-\frac{4\pi}{\nu A_\nu}\int_0^1[x^2G'(x)]'dx=-\frac{4\pi}{\nu A_\nu}G'(1^-).$$

However, $C_\nu=-G'(1^-)$ which completes the proof of the lemma. □

The velocity flow can be described around the edge of the hotspot

$$u(t,r)=R_h'(t)-\frac{C_\nu\overline{\chi}T_c(t)^\nu T_\infty(t)}{\nu\gamma pR_h(t)}f\left(\frac{r-R_h(t)}{D(t)}\right). \tag{31}$$

To lowest order in δ the velocity is $R_h'(t)$. The correction is of order δ. This correction is important in that it is the one that is related to ablation. By denoting by $\rho_\infty(t)$ the shell density and by defining the ablation velocity $V_a(t)$ by the identity $\rho_\infty(t)V_a(t)=$mass flow$=\rho_{loc}(t)V_{loc}(t)$, we get a closed form expression for the ablation velocity

$$V_a(t)=-\frac{C_\nu\chi}{\nu\gamma c_v}\frac{T_c(t)^\nu}{R_h(t)\rho_\infty(t)}. \tag{32}$$

The density-gradient scale length is $L_g=|\rho/\partial_r\rho|$. From the differential equation satisfied by g it is easy to establish that the minimum density-gradient scale length is reached at the point where the temperature value is $T=[(\nu+1)/\nu]T_\infty(t)$, and then

$$L_{g,min}(t)=\frac{(\nu+1)^{\nu+1}}{C_\nu\nu^{\nu-1}}\left(\frac{T_\infty(t)}{T_c(t)}\right)^\nu R_h(t),$$

where $(\nu+1)^{\nu+1}/(C_\nu\nu^{\nu-1})\simeq 6.86$ for $\nu=5/2$. Note that this result is consistent with the one obtained by Kull with the well known isobaric model.[11] The expressions of the ablation velocity and the minimum density-gradient length scale are important because they play key roles in the growths of RT instabilities, as we shall see in Sec. VI.

V. SHELL MODELS

The previous sections demonstrate that local and global hydrodynamic quantities are functions of the hotspot pressure $p(t)$. Additional equations must be exhibited to close the system. These equations result from the coupling of the hotspot with the shell surrounding the hotspot. A first model consists in approximating the shell by a thin and incompressible layer of high-density material.[2] The shell motion is then deduced from Newton's law which provides the additional equation required to close the system. This simple model was analyzed in Ref. 2 but as discussed in Ref. 3 the comparisons with numerical simulations do not exhibit good agreement. The main reason is that shells are thick and compressible in ICF. Furthermore, a return shock is created at the edge of the hotspot and travels through the shell, which is not a uniform medium anymore but exhibits two regions with different characteristics. In Ref. 3 a thick shell model is introduced and results are proposed and discussed without derivation. The goal of this section is to derive and generalize this model. In particular we derive the equations for arbitrary

adiabatic exponents in the gaseous hotspot and the solid shell, and we consider a different profile for the free-falling shell material. We also discuss the validity of the model by pointing out the underlying hypotheses.

A. The thick shell model

An accurate model should take into account the return shock in the cold unperturbed shell. The deceleration phase actually starts when the shock reflected from the center of the capsule interacts with the incoming shell. We thus consider that the shock starts at time 0 from the edge of the hotspot and propagates within the shell. We denote by R_s the location of the shock. Three regions can be distinguished which are as follows:

(1) $r<R_h(t)$ corresponds to the hotspot.
(2) $R_h(t)<r<R_s(t)$ corresponds to the shocked shell.
(3) $r>R_s(t)$ corresponds to the cold unperturbed shell, whose pressure is much lower.

Let us first consider the outer region $r>R_s(t)$. The shell is in free-fall conditions, with an evanescent pressure. This region is not yet perturbed by the hotspot. By assuming a uniform implosion velocity profile and by integrating the equations of motion in spherical geometry, we get with an evanescent pressure and heat conductivity that, for $r>R_s(t)$,

$$u_{\rm ff}(t,r) = -V_i, \tag{33}$$

$$\rho_{\rm ff}(t,r) = \frac{M_{\rm sh}}{4\pi r^2 \Delta_0}\overline{\rho_0}\left(\frac{r+V_i t - R_0}{\Delta_0}\right), \tag{34}$$

where V_i is the implosion velocity, $M_{\rm sh}$ is the initial shell mass, R_0 is the initial location of the shell inner surface, and Δ_0 is the initial shell thickness. The normalized density profile $\overline{\rho_0}$ is such that $\overline{\rho_0}(x)=0$ for $x\leqslant 0$, $\overline{\rho_0}(x)>0$ for $x>0$, and $\int_0^\infty \overline{\rho_0}(x)dx=1$.

The shock propagation is governed by the Rankine–Hugoniot relations[12]

$$[\rho u] = R_s'[\rho],$$

$$[p+\rho u^2] = R_s'[\rho u],$$

$$\left[\gamma_s p u + \frac{\gamma_s-1}{2}\rho u^3\right] = R_s'\left[p+\frac{\gamma_s-1}{2}\rho u^2\right].$$

We denote by γ_s the adiabatic exponent in the shell in contrast with the value γ_g in the gaseous hotspot. In front of the shock the pressure is evanescent, so we have $p(R_s^+)\simeq 0$, $u(R_s^+)=u_{\rm ff}(R_s,t)$, $\rho(R_s^+)=\rho_{\rm ff}(R_s,t)$. Behind the shock the pressure, velocity, and density are denoted by $p_s(t)=p(R_s^-,t)$, $v_s(t)=u(R_s^-,t)$, and $\rho_s(t)=\rho(R_s^-,t)$. Substituting into the Rankine–Hugoniot relations we obtain

$$\rho_s(t) = \rho_{\rm ff}(R_s,t)\frac{\gamma_s+1}{\gamma_s-1},$$

$$p_s(t) = \rho_{\rm ff}(R_s,t)[v_s - u_{\rm ff}(R_s,t)][R_s' - u_{\rm ff}(R_s,t)],$$

$$R_s'(t) = -\frac{\gamma_s-1}{2}u_{\rm ff}(R_s,t) + \frac{\gamma_s+1}{2}v_s.$$

In the shocked shell region $R_h<r<R_s$ the dynamics is governed by the equations of motion (1)–(3) in absence of heat conduction and nuclear reaction. We cannot assume anymore a subsonic flow, so that these equations are equivalent to Euler equations. Let us introduce the shocked shell mass

$$M_{\rm ss} = 4\pi\int_{R_h}^{R_s}\rho r^2 dr.$$

The hotspot mass is negligible with respect to the shell mass, so the integration domain can be set to $[0,R_s]$ with a negligible error. By differentiating this identity and using the mass conservation equation we find $M_{\rm ss}'=4\pi R_s^2\rho_s(t)(R_s'-v_s)$. From the expression of $\rho_s(t)$ in terms of $\rho_{\rm ff}$ we get

$$M_{\rm ss}' = 4\pi R_s^2\rho_{\rm ff}(t,R_s)[R_s' - u_{\rm ff}(t,R_s)]. \tag{35}$$

We introduce the average velocity of the shocked shell

$$U_{\rm ss} = \frac{4\pi\langle\rho u\rangle}{M_{\rm ss}}, \quad \langle\rho u\rangle = \int_{R_h}^{R_s}\rho u r^2 dr.$$

Once again, as the hotspot mass is much smaller than the shell mass, we can set the integration domain to $[0,R_s]$. We then differentiate $\langle\rho u\rangle$ and use the momentum conservation equation and the expressions of ρ_s, v_s, and p_s. We obtain

$$\langle\rho u\rangle' = \rho_{\rm ff}(t,R_s)u_{\rm ff}(t,R_s)[R_s' - u_{\rm ff}(t,R_s)] + 2\int_0^{R_s} p r dr.$$

The first term in the right-hand side can be expressed in terms of $M_{\rm ss}'$. The second term can also be simplified because the volume inside R_s is occupied mostly by the hotspot. This is equivalent to assume $R_s-R_h\ll R_h$, which holds true at the beginning of the deceleration phase, but has to be checked *a posteriori* during the whole phase. As a result the second term can be approached by $2\int_0^{R_h} p r dr$. Furthermore the pressure is almost uniform in the hotspot so that we finally obtain

$$4\pi\langle\rho u\rangle' = M_{\rm ss}'u_{\rm ff}(t,R_s) + pR_h^2.$$

The average velocity thus satisfies

$$(M_{\rm ss}U_{\rm ss})' = M_{\rm ss}'u_{\rm ff}(t,R_s) + 4\pi p R_h^2. \tag{36}$$

The velocity profile is not easy to compute because all quantities in the Euler equations are of the same order in the shocked shell. Consistently with the hypothesis $R_s-R_h\ll R_h$, we assume that the fluctuations of the velocity flow inside the shocked shell $R_h<r<R_s$ are small and we accordingly adopt the uniform profile $u(t,r)=R_h'(t)$. We shall see in the following section another model that takes into account an affine variation of the velocity flow. In case of a uniform profile we have $v_s(t)=R_h'(t)$ and the average velocity is $U_{\rm ss}(t)=R_h'(t)$ as well. By grouping the last identity with Eqs.

(35) and (36) and by introducing the velocity of the shell inner surface $U_h = R_h'(t)$, we get a system of five differential equations with five unknown variables $(R_s, R_h, U_h, M_{ss}, p)$. By choosing a model for the flow in the free-fall shell, the system can be closed and integrated. Let us adopt the model (33) and (34). We introduce dimensionless variables $\overline{R_s} = R_s/R_0$, $\overline{R_h} = R_h/R_0$, $\overline{U_h} = U_h/V_i$, $\overline{p} = p/p_0$, $\overline{M_{ss}} = M_{ss}/M_{sh}$, and $\tau = V_i t/R_0$ so that the system reads as $\overline{R_h'} = \overline{U_h}$,

$$\overline{U_h'} = \frac{1}{\hat{\epsilon}_0}\frac{\overline{R_h^2}\,\overline{p}}{\overline{M_{ss}}} - \frac{\overline{M_{ss}'}}{\overline{M_{ss}}}[\overline{U_h} + 1],$$

$$\overline{R_s'} = \frac{\gamma_s - 1}{2} + \frac{\gamma_s + 1}{2}\overline{U_h},$$

$$\overline{M_{ss}'} = A_0(1 + \overline{R_s'})\overline{\rho_0}[A_0(\overline{R_s} + \tau - 1)],$$

$$\overline{p'} = -3\gamma_g\frac{\overline{U_h}}{\overline{R_h}}\overline{p} + \frac{Y_\alpha}{\hat{\epsilon}_0^2}\overline{p},$$

with the initial conditions $\overline{R_s}(0) = 1$, $\overline{R_h}(0) = 1$, $\overline{U_h}(0) = 0$, $\overline{M_{ss}}(0) = 0$, and $\overline{p}(0) = 1$. In the above equations the prime indicates a derivative with respect to τ. This analysis shows that there are only three independent parameters

$$\hat{\epsilon}_0 = \frac{M_{sh}V_i^2}{4\pi p_0 R_0^3}, \quad Y_\alpha = \frac{\mu_\alpha p_0 R_0}{V_i}\hat{\epsilon}_0^2, \quad A_0 = \frac{R_0}{\Delta_0}. \tag{37}$$

$\hat{\epsilon}_0$ is proportional to the ratio of the initial kinetic energy of the shell over the initial internal energy of the hotspot. A_0 is the initial shell aspect ratio. Y_α characterizes the reaction rate.

B. Refinement of the thick shell model

In the preceding section we have assumed a uniform profile for the velocity flow inside the shocked shell $R_h(t) < r < R_s(t)$. In this section we refine this model by assuming an affine function for the velocity profile. Taking into account $u[t, R_h(t)] = R_h'(t)$ we write

$$u(r,t) = R_h'(t) + \frac{r - R_h(t)}{R_s(t) - R_h(t)}[v_s(t) - R_h'(t)]. \tag{38}$$

Using the energy conservation equation and the relation $u[t, R_h(t)] = R_h'(t)$, the slope of u at R_h can be identified

$$\frac{\partial u}{\partial r}[t, R_h(t)] = -\frac{p'}{\gamma_s p}(t) - 2\frac{R_h'}{R_h}(t).$$

Comparing with Eq. (38) we get the expression of v_s which can be simplified using Eq. (9)

$$v_s(t) = R_h'(t) + \alpha(t)[R_s(t) - R_h(t)], \tag{39}$$

where

$$\alpha(t) = \left(3\frac{\gamma_g}{\gamma_s} - 2\right)\frac{R_h'}{R_h}(t) - \frac{\mu_\alpha}{\gamma_s}p(t).$$

We finally rewrite the velocity profile (38) with this additional identity and get $u(t,r) = R_h'(t) + \alpha(t)[r - R_h(t)]$.

We shall use the mass conservation equation to get the density profile. Let us introduce $\tilde{\rho}(t,r) = r^2\rho[t, r + R_s(t)]$ and $\tilde{u}(t,r) = u[t, r + R_s(t)]$. Taking into account the velocity profile that we have just derived, $\tilde{\rho}$ satisfies

$$\frac{\partial\tilde{\rho}}{\partial t} + \left(v_s - R_s' + \frac{v_s - R_h'}{R_s - R_h}r\right)\frac{\partial\tilde{\rho}}{\partial r} + \frac{v_s - R_h'}{R_s - R_h}\tilde{\rho} = 0,$$

with the initial condition at $r = 0$: $\tilde{\rho}(t, r = 0) = R_s^2(t)\rho_s(t)$. The solution can be computed explicitly and turns out to be an affine function

$$r^2\rho(t,r) = \{R_s^2\rho_s(t) + [r - R_s(t)]\beta(t)\} \tag{40}$$

β can be identified easily as a function of the shocked shell mass M_{ss}. We get

$$\beta(t) = \frac{R_s^2\rho_s(t)}{R_s(t) - R_h(t)} - \frac{M_{ss}(t)}{2\pi[R_s(t) - R_h(t)]^2}.$$

We now express the average shocked shell velocity U_{ss} as a function of the other quantities. Let us denote $\breve{\rho}(t,r) = \rho(t,r)r^2$. In the shocked shell region the velocity u and density $\breve{\rho}$ are affine functions. By integrating these functions we get

$$U_{ss}(t) = u_{1/2}(t)\left[1 + \frac{\alpha(t)\beta(t)}{12u_{1/2}(t)\breve{\rho}_{1/2}(t)}(R_s - R_h)^2\right],$$

where $\breve{\rho}_{1/2}(t)$ and $u_{1/2}(t)$ are the values of $\breve{\rho}$ and u at $[R_h(t) + R_s(t)]/2$. However, α and β are of the same order as $u_{1/2}/R_h$ and $\breve{\rho}_{1/2}/(R_s - R_h)$, respectively. By using the assumption that the thickness $R_s - R_h$ of the shocked shell is smaller than R_h, we can safely make the approximation $U_{ss} \simeq u_{1/2}$. By Eq. (38) we thus have $U_{ss} = [v_s(t) + R_h'(t)]/2$. Combining with Eq. (39) yields

$$U_{ss}(t) = R_h'(t) + \frac{\alpha(t)}{2}[R_s(t) - R_h(t)]. \tag{41}$$

By grouping Eqs. (9), (35), (36), and (41), and by introducing the velocity at the edge of the hotspot $U_h = R_h'(t)$, we get a system of five first-order differential equations with five unknown variables $(R_s, R_h, U_h, M_{ss}, p)$. By choosing the free model (33) and (34) for the shell, we get a closed system describing the shell and the hotspot. We introduce dimensionless variables $\overline{R_s} = R_s/R_0$, $\overline{R_h} = R_h/R_0$, $\overline{U_h} = U_h/V_i$, $\overline{p} = p/p_0$, $\overline{M_{ss}} = M_{ss}/M_{sh}$, and $\tau = V_i t/R_0$ so that the system reads as $\overline{R_h'} = \overline{U_h}$,

$$\overline{R_s'} = \frac{\gamma_s - 1}{2} + \frac{\gamma_s + 1}{2}\left\{\overline{U_h} + \left[\left(3\frac{\gamma_g}{\gamma_s} - 2\right)\frac{\overline{U_h}}{\overline{R_h}} - \frac{Y_\alpha}{\gamma_s\hat{\epsilon}_0^2}\overline{p}\right][\overline{R_s} - \overline{R_h}]\right\},$$

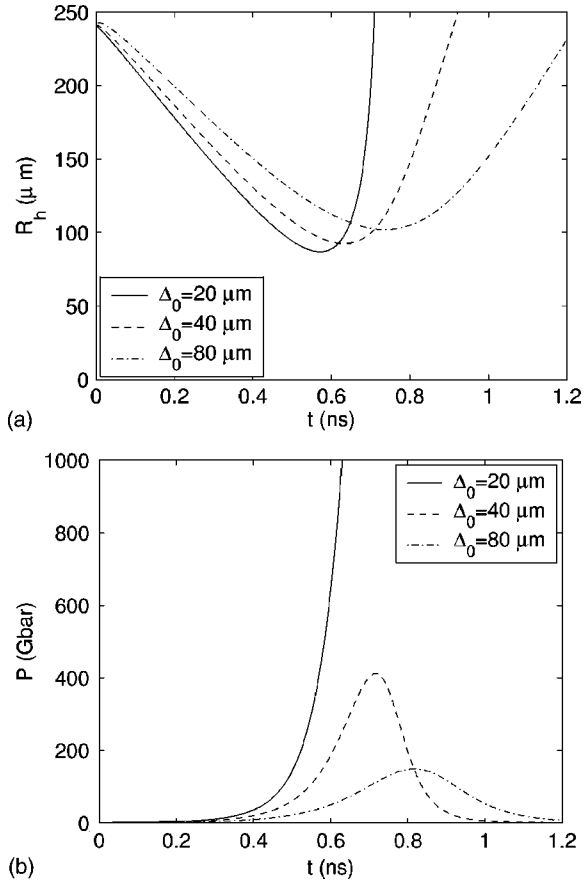

FIG. 2. Time evolutions of the hotspot radius (a) and pressure (b) for the NIF capsule. The thick shell model is numerically integrated for different values of the initial shell thickness.

$$\overline{U_h'} = \frac{\overline{R_h}}{\overline{R_h}\left(2-\frac{3\gamma_g}{2\gamma_s}\right)+\overline{R_s}\left(\frac{3\gamma_g}{2\gamma_s}-1\right)}\left(\left(1-\frac{3\gamma_g}{2\gamma_s}\right)\right.$$
$$\times\overline{U_h}\frac{\overline{R_s'}\,\overline{R_h}-\overline{R_s}\,\overline{U_h}}{\overline{R_h^2}}+\frac{Y_\alpha}{2\gamma_s\hat{\epsilon}_0^2}[\overline{p'}(\overline{R_s}-\overline{R_h})$$
$$+\overline{p}(\overline{R_s'}-\overline{U_h})]+\frac{1}{\hat{\epsilon}_0}\frac{\overline{R_h^2}\,\overline{p}}{\overline{M_{ss}}}-\frac{\overline{M_{ss}'}}{\overline{M_{ss}}}\left\{\overline{U_h}+1\right.$$
$$\left.\left.+\left[\left(\frac{3\gamma_g}{2\gamma_s}-1\right)\frac{\overline{U_h}}{\overline{R_h}}-\frac{Y_\alpha}{2\gamma_s\hat{\epsilon}_0^2}\overline{p}\right](\overline{R_s}-\overline{R_h})\right\}\right),$$

$$\overline{M_{ss}'} = A_0(1+\overline{R_s'})\overline{\rho_0}[A_0(\overline{R_s}+\tau-1)],$$

$$\overline{p'} = -3\gamma_g\frac{\overline{U_h}}{\overline{R_h}}\overline{p}+\frac{Y_\alpha}{\hat{\epsilon}_0^2}\overline{p},$$

with the initial conditions $\overline{R_s}(0)=1$, $\overline{R_h}(0)=1$, $\overline{U_h}(0)=0$, $\overline{M_{ss}}(0)=0$, and $\overline{p}(0)=1$. The three parameters of the problem are Eq. (37). If $\Delta_0\to 0$ then we recover the thin shell model. As soon as $\Delta_0>0$, the pressure and acceleration are reduced compared to the thin shell model. This is due to the fact that only the shocked shell part acts as a piston while the return shock has not crossed the whole shell.

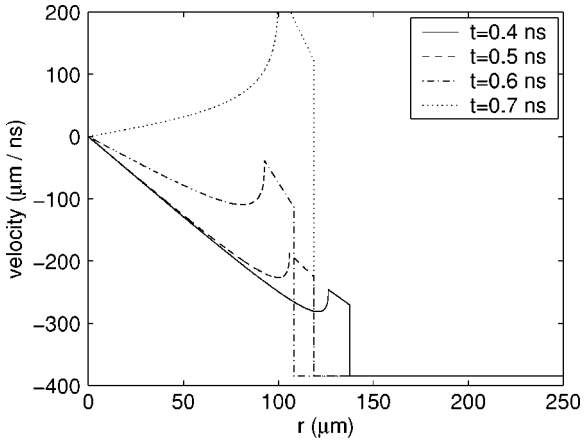

FIG. 3. Velocity profiles for the NIF capsule, $\Delta_0=40$ μm.

We consider the averaged parameters at the beginning of the deceleration phase for the direct-drive NIF-like capsule studied in Ref. 2: $M_{sh}=1.1$ mg, $p(0)=0.9$ Gbar, $R_h(0)=240$ μm, $V_i=385$ μm/ns. We assume a density profile for the free-falling shell material of the type $\overline{\rho_0}(x)=4x^2\exp(-2x)$. We also have $c_v=10^4$ m^2 s^{-2} K^{-1}, $\chi=6\times10^{-8}$ m g s^{-3} K^{-7}, $\gamma_g=5/3$, and $\gamma_s=7/4$. Finally $\mu_\alpha=\theta\,9.12\times10^{-10}$ m s g^{-1}, with θ the absorbed α-particle fraction. We plot in Fig. 2 the time evolutions of hotspot radius and pressure in the case $\theta=40\%$. We consider different values for the initial shell thickness, which shows that the thin shell model $\Delta_0\ll R_0$ is too optimistic as pointed out in Ref. 3.

The velocity profile is plotted in Fig. 3 at different times. The three main regions can be distinguished: hotspot $r<R_h(t)$, shocked shell $R_h(t)<r<R_s(t)$, and free-fall shell $r>R_s(t)$. The velocity profile is given by Eq. (15) in the part $r<R_h(t)$, by the affine profile (38) in the part $R_h(t)<r<R_s(t)$, and by the free-fall velocity $-V_i$ in the part $r>R_h(t)$. In particular, we can check *a posteriori* the hypothesis about the small fluctuations of the velocity profile inside the shocked shell.

In the same way we study the nominal indirectly driven LMJ capsule.[13] At the beginning of the deceleration phase we have $M_{sh}=0.31$ mg, $p(0)=0.6$ Gbar, $R_h(0)=120$ μm, $V_i=390$ μm/ns, and $\Delta_0=80$ μm. We plot in Fig. 4 the evolutions of the hotspot radius and pressure for different values of the absorbed α-particle fraction. If $\theta\geqslant 78\%$, then the solution blows up in finite time, which means that the quadratic approximation for the fusion cross section is not valid anymore. This blow-up can also be interpreted as the ignition of the capsule. The thick shell model can thus be used as a simplified model for the determination of ignition criteria.

VI. HYDRODYNAMIC INSTABILITIES

A rough estimate of the linear RT growth rates for large l modes can be obtained by using well-known planar results.[2,14] However a more accurate model should take into account spherical convergence effects.

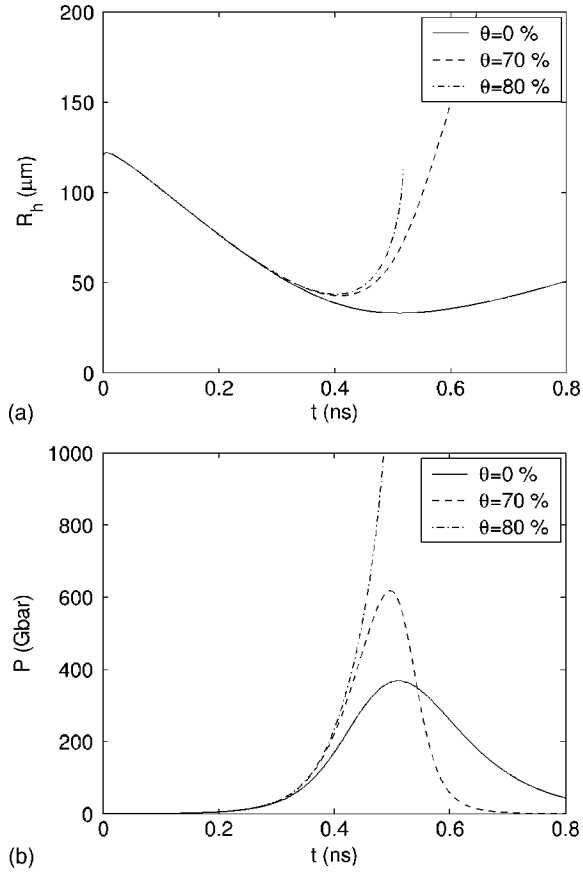

FIG. 4. Time evolutions of the hotspot radius (a) and pressure (b) for the LMJ capsule. The thick shell model is numerically integrated for different absorbed α-particle fractions θ.

Unperturbed state. We consider a simplified model where the density of the unperturbed state is uniform in each region delimited by the interface $r=R_h(t)$. By integrating the mass conservation equation in each region

$$u_I(t,r) = -\frac{\rho_I'}{3\rho_I} r, \tag{42}$$

$$u_E(t,r) = -\frac{\rho_E'}{3\rho_E} r + \frac{R_h^2}{r^2}\left(R_h' + \frac{R_h}{3}\frac{\rho_E'}{\rho_E} + v_E\right), \tag{43}$$

where subscript E (resp. I) denotes the external outer (resp. inner) region. Jump conditions impose

$$[\rho_0 v_0] = 0, \quad [p_0 + \rho_0 v_0^2] = 0, \tag{44}$$

where $u_I[t,R_h(t)^-] = R_h'(t) + v_I(t)$ and $u_E(t,R_h(t)^+) = R_h'(t) + v_E(t)$. We denote the mass flow by $\dot{m} = \rho_E v_E = \rho_I v_I$. In the following we carry out the stability analysis of this hydrodynamic configuration. The perturbed interface is parameterized as $r = R_h(t) + \eta_1(t,\theta,\phi)$. We expand all hydrodynamic variables in the inner and outer regions as $u = u_0 + u_1, \ldots$ with u_0 given by Eqs. (42) and (43) and we consider the linearized evolution problem for the perturbed variables $u_1, \ldots$, and η_1.

Perturbed jump conditions. The stability of solutions of nonlinear hyperbolic systems of conservation laws has been studied in Ref. 15. Rankine–Hugoniot relations for the perturbed hydrodynamic variables can be expressed in absence of density perturbation as

$$R_h^2[\rho_0 u_{r1}] = [\partial_t(R_h^2 \rho_0 \eta_1)], \tag{45}$$

$$R_h^2[p_1 + 2\dot{m}u_{r1}] = [\rho_0] R_h^2 R_h'' \eta_1 + 2\dot{m}[v_0] R_h \eta_1, \tag{46}$$

$$R_h[u_{\theta 1}] = -[v_0]\partial_\theta(\eta_1), \tag{47}$$

$$R_h \sin(\theta)[u_{\phi_1}] = -[v_0]\partial_\phi(\eta_1). \tag{48}$$

Assuming that the interface is an isotherm we get the supplementary jump condition[16]

$$[u_{r_1}] + \eta_1[\partial_r u_0] = -\eta_1[v_0]\frac{\partial_r \psi}{\psi}(R_h),$$

where ψ is a solution to the Laplace equation $\Delta\psi = 0$. The partial derivatives $\partial_r u_0$ can be evaluated from the unperturbed velocity profiles. Besides, in spherical geometry and in the case of a single-mode perturbation we have $\psi = r^l$ so that the supplementary jump condition reads as

$$[u_{r_1}] = \eta_1\left[\frac{\rho_0'}{\rho_0}\right] - \frac{l-2}{R_h}\eta_1[v_0]. \tag{49}$$

Linearized perturbed system. The linearized mass conservation equation reads $\partial_t(\rho_1/\rho_0) + u_0\partial_r(\rho_1/\rho_0) = 0$. Using the arguments of Refs. 16 and 17 we neglect density perturbations and put $\rho_1 = 0$. The momentum and energy equations in spherical coordinates take the form

$$\partial_t(u_{r_1}) + \partial_r(u_0 u_{\theta_1}) + \partial_r\left(\frac{p_1}{\rho_0}\right) = 0,$$

$$\partial_t(u_{\theta_1}) + \frac{u_0}{r}\partial_r(r u_{\theta_1}) + \frac{1}{r}\partial_\theta\left(\frac{p_1}{\rho_0}\right) = 0,$$

$$\partial_t(u_{\phi_1}) + \frac{u_0}{r}\partial_r(r u_{\phi_1}) + \frac{1}{r\sin(\theta)}\partial_\phi\left(\frac{p_1}{\rho_0}\right) = 0,$$

$$\partial_r(r^2 u_{r_1}) + \frac{r}{\sin(\theta)}\{\partial_\theta[\sin(\theta)u_{\theta_1}] + \partial_\phi(u_{\phi_1})\} = 0.$$

Solution in the outer region. The vorticity created by the instability at the interface is not convected toward this region so that we can consider that the flow is irrotational. Introducing the velocity potential $\mathbf{u}_1 = \boldsymbol{\nabla}\psi_1$ the linearized energy conservation equation imposes the Laplace equation $\Delta\psi_1 = 0$. By considering a single-mode perturbation (l,m), the general solution that does not blow up at infinity is $\psi_1(t,r,\theta,\phi) = d(t) r^{-l-1} P_l^m[\cos(\theta)] e^{im\phi}$. The perturbation of the pressure is given by $-p_1/\rho_0 = \partial_t\psi_1 + u_0\partial_r\psi_1$. The perturbations of the velocity and pressure are thus of the form

$$u_{r_1}(t,r,\theta,\phi) = \tilde{u}_{r_1}(t,r) P_l^m[\cos(\theta)] e^{im\phi}, \tag{50}$$

$$u_{\theta_1}(t,r,\theta,\phi) = \tilde{u}_{\theta_1}(t,r)\partial_\theta P_l^m[\cos(\theta)] e^{im\phi}, \tag{51}$$

$$u_{\phi_1}(t,r,\theta,\phi) = \tilde{u}_{\phi_1}(t,r)\frac{im}{\sin(\theta)}P_l^m[\cos(\theta)]e^{im\phi}, \tag{52}$$

$$p_1(t,r,\theta,\phi) = \tilde{p}_1(t,r)P_l^m[\cos(\theta)]e^{im\phi}, \tag{53}$$

where $\tilde{u}_{\phi_1}=\tilde{u}_{\theta_1}$,

$$\tilde{u}_{r_1}[t,R_h(t)^+] = \frac{D}{R_h}(t), \tag{54}$$

$$\tilde{u}_{\theta_1}[t,R_h(t)^+] = -\frac{D}{(l+1)R_h}(t), \tag{55}$$

$$\tilde{p}_1[t,R_h(t)^+] = \rho_E(t)\left(\frac{D'}{l+1} - \frac{v_E}{R_h}D\right)(t). \tag{56}$$

$D(t)=-(l+1)d(t)R_h(t)^{-l-1}(t)$ is an arbitrary function.

Solution in the inner region. The vorticity denoted by $\omega=\boldsymbol{\nabla}\times\mathbf{u}_1$ is convected from the interface toward this region. The evolution equation of ω_r combined with a vanishing initial condition establishes that $\omega_r=0$. The ϕ component is found to satisfy

$$[\partial_t + u_0\partial_r + (\partial_r u_0)](r\omega_\phi) = 0. \tag{57}$$

Using the linearized conservation equations we get that $\mathbf{u}_1$ and p_1 can be written in the form (50)–(53), so that ω_ϕ reads as

$$\omega_\phi(t,r,\theta,\phi) = \tilde{\omega}_\phi(t,r)\partial_\theta P_l^m[\cos(\theta)]e^{im\phi},$$

while the radial velocity and the ϕ component of the vorticity satisfy the differential equation

$$\partial_r^2(r^2\tilde{u}_{r_1}) - l(l+1)\tilde{u}_{r_1} = l(l+1)r\tilde{\omega}_\phi. \tag{58}$$

Equation (57) imposes that $\tilde{\omega}_\phi(t,r)=\rho_I(t)rF[\rho_I(t)r^3]$ where F is an arbitrary function. The solution to Eq. (58) bounded at 0 then reads as

$$\tilde{u}_{r_1}(t,r) = a(t)r^{l-1} + \frac{l(l+1)}{3(2l+1)r}\int_0^\xi \left(\frac{s}{\xi}\right)^{-l/3}F(s)ds - \frac{l(l+1)}{3(2l+1)r}\int_0^\xi \left(\frac{s}{\xi}\right)^{(l+1)/3}F(s)ds,$$

where $\xi(t,r)=\rho_I(t)r^3$. By substitution we get the expressions of the other components of the perturbed velocity and pressure. Finally, let us introduce

$$A(t) = a(t)R_h^l(t),$$

$$B(t) = \frac{l(l+1)}{3(2l+1)}\int_0^{\xi(t)}\left(\frac{s}{\xi(t)}\right)^{-l/3}F(s)ds,$$

$$C(t) = -\frac{l(l+1)}{3(2l+1)}\int_0^{\xi(t)}\left(\frac{s}{\xi(t)}\right)^{(l+1)/3}F(s)ds,$$

where $\xi(t)=\rho_I(t)R_h(t)^3$, the perturbations of the velocity $\mathbf{u}_1$ and pressure p_1 can be written as

$$\tilde{u}_{r1}[t,R_h(t)^-] = \frac{A}{R_h} + \frac{B}{R_h} + \frac{C}{R_h}, \tag{59}$$

$$\tilde{u}_{\theta 1}[t,R_h(t)^-] = \frac{1}{l}\left(\frac{A}{R_h} + \frac{B}{R_h}\right) - \frac{1}{l+1}\frac{C}{R_h}, \tag{60}$$

$$\tilde{p}_1[t,R_h(t)^-] = -\rho_I(t)\left(\frac{A'}{l} + \frac{v_I}{R_h}A\right), \tag{61}$$

and $\tilde{u}_{\phi_1}=\tilde{u}_{\theta_1}$. Note that three parameters appear, but there are actually only two free parameters because by differentiating $B+C$ we get the additional identity

$$\frac{C}{l+1} - \frac{B}{l} = -\left(\frac{\rho_I'}{3\rho_I} + \frac{R_h'}{R_h}\right)^{-1}\frac{(B+C)'}{l(l+1)} - \frac{B+C}{l(l+1)}. \tag{62}$$

Interface motion. We substitute the expressions of the modes (54)–(56) and (59)–(61) into the jump conditions (45)–(49). Combining with Eq. (62) we get a system of four equations with four unknowns A, $B+C$, D, and η_1. We thus get a compatibility equation that governs the growth of η_1. Taking into account $\rho_E \gg \rho_I$ the interface motion in terms of the rescaled elevation $\tilde{\eta}_1=R_h^2\rho_E\eta_1$ can be written as a second-order differential equation

$$\tilde{\eta}_1'' + \kappa_1\tilde{\eta}_1' + \left(\kappa_2 - A_t\frac{l+1}{R_h}R_h''\right)\tilde{\eta}_1 = 0, \tag{63}$$

$$\kappa_1 = -\frac{4l^2-1}{lR_h}v_E - \frac{R_h'}{R_h} - \frac{\rho_E'}{\rho_E},$$

$$\kappa_2 = v_E\left[\frac{(l^2+l+7)(l+1)}{lR_h^2}v_I + \frac{7l^2+6l+5}{lR_h}\frac{R_h'}{R_h} + \frac{3l^2+l+1}{lR_h}\frac{\rho_E'}{\rho_E} - \frac{2l^2-3l-2}{lR_h}\frac{v_E'}{v_E}\right],$$

$$A_t = \frac{v_I - v_E}{v_I + v_E}.$$

The first terms of κ_1 and κ_2 are standard and correspond to ablative stabilization. The other terms are imposed by convergence effects. The ablation velocity v_E, the shell density ρ_E, the interface position R_h and velocity R_h' are well-defined quantities. The inner velocity v_I should be expressed in terms of the other parameters to get a closed system. The self-consistent analysis proposed in Ref. 17 establishes that accurate results are obtained when choosing

$$v_I(t) = \frac{v_E(t)}{\mu_\nu}\left(\frac{1}{k(t)L_0(t)} + K_\nu\right)^{1/\nu},$$

where $k(t)=l/R_h(t)$ and L_0 is proportional to the minimal density-gradient length scale. For $\nu=5/2$ we have $\mu_\nu=1.05$, $K_\nu=1.57$, and $L_0=0.12L_{g,min}$.

Assuming that the parameters of the shell implosion are slowly varying over the time studied, we may assume a solution of the form $\eta_1(t)=\eta_1(0)\exp(\gamma_{\mathrm{RT}}t)$ where γ_{RT} is the linear RT growth rate, and Eq. (63) can be reduced to a second-order polynomial, which gives

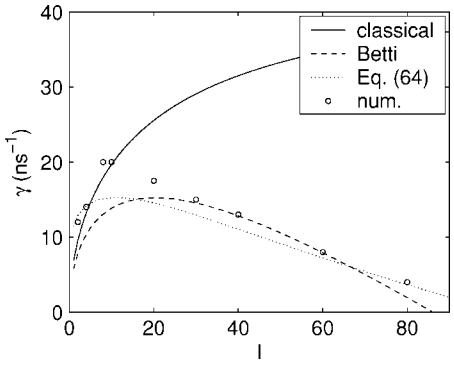

FIG. 5. RT growth rate vs mode number for the deceleration phase of a NIF-like capsule as predicted by this work [Eq. (64)] and by reference formulas neglecting convergence effects. These theoretical predictions are compared with numerical results addressing this capsule (Ref. 3).

$$\gamma_{\mathrm{RT}} = \sqrt{A_t(l+1)R_h''/R_h + \kappa_1^2/4 - \kappa_2} - \frac{\kappa_1}{2} - 2\frac{R_h'}{R_h} - \frac{\rho_E'}{\rho_E}. \quad (64)$$

Let us consider the direct-drive NIF-like capsule studied in Ref. 3 in the last moments (the last 100 ps) before stagnation. The authors give $R_h'' \simeq 3100\ \mu\mathrm{m/ns}^2$, $v_E \simeq -18\ \mu\mathrm{m/ns}$, $L_{g,min} \simeq 1.5\ \mu\mathrm{m}$, $R_h \simeq 65\ \mu\mathrm{m}$, leading to a Froude number $\mathrm{Fr} \simeq 0.5$. We also take $\nu = 5/2$ and the implosion velocity is typically around $R_h' = -200\ \mu\mathrm{m/ns}$. Feeding Eq. (64) with these data, we can compute the RT growth rate of η_1. Figure 5 compares our result with the classical fitting formula $\sqrt{kR_h''/(1+kL_{g,min})}$, $k = l/R_h$, and the formula (61) (Ref. 3) obtained by Betti *et al.* taking into account ablation, thermal conduction, finite density gradient, but neglecting convergence effects, $0.9\sqrt{kR_h''/(1+kL_{g,min})} - 1.4k|v_E|$. The results of numerical simulations given in Ref. 3 are also reported. This shows that the cutoff mode number is $l \simeq 100$, and that spherical convergence effects induce slight enhancements of the RT growth rates for low modes $l \leqslant 20$. Note, however, that the RT growth rates vary strongly with the implosion velocity and acceleration, so that comparisons with numerical simulations are not easy.

Let us finally consider the nominal indirectly driven LMJ capsule. In the last 50 ps before stagnation we have $R_h'' \simeq 1000\ \mu\mathrm{m/ns}^2$, $v_E \simeq -15\ \mu\mathrm{m/ns}$, $L_{g,min} \simeq 1.5\ \mu\mathrm{m}$, $R_h \simeq 40\ \mu\mathrm{m}$ leading to a Froude number $\mathrm{Fr} \simeq 0.6$. The implosion velocity is typically around $R_h' = -100\ \mu\mathrm{m/ns}$. The growth rate is plotted in Fig. 6, and we find that the cutoff mode number is $l \simeq 30$. We expect to be able to perform numerical simulations in the near future for this case and to get the growth rates of low modes. The overall result with the considered data is that the linear deceleration-phase RT growth rates for the indirectly driven LMJ capsule are smaller than the ones of the direct-drive NIF-like capsule.

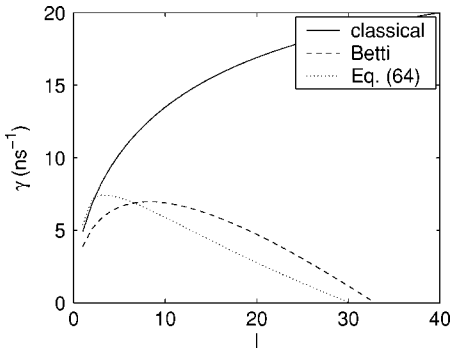

FIG. 6. RT growth rate vs mode number for the deceleration phase of the LMJ capsule.

VII. CONCLUSION

We have carried out a multiscale analysis of the hotspot during the deceleration phase of ICF capsules which gives information at a macroscopic level, useful for ignition criteria for instance, as well as microscopic detail, necessary for the computations of RT growth rates. We have shown that the flow inside the hotspot converges towards a self-similar profile whose dynamics depends on the hotspot uniform pressure. We have exhibited that the hotspot is separated from the shell by a thin layer that also possesses a microscopic self-similar profile. The derivation of a closed system requires the coupling of the flows inside the hotspot and in the shell. We have discussed and generalized a thick shell model originally proposed by Betti *et al.*[3] that takes into account the return shock that propagates through the shell. As a result we have derived a closed system of ordinary differential equations governing the hotspot and shell dynamics. Finally we have computed the linear growth rates of the deceleration phase RT instability taking into account the stabilizing ablation and the spherical convergence.

ACKNOWLEDGMENTS

The authors thank P.-A. Raviart and L. Masse for useful and stimulating discussions.

APPENDIX: PROOF OF EQ. (22)

We prove in this Appendix the convergence of the macroscopic temperature profile to the self-similar solution. We first introduce some notations. If $a < b$ and $g:(a,b) \to \mathbf{R}^+$ is a positive-valued function, then we introduce the Hilbert space $L^2[g(x)dx]$ equipped with the weighted norm

$$\|f\|^2_{g(x)dx} = \int_a^b f^2(x)g(x)dx.$$

Proof of Eq. (22) with $(\mu^{(a)}, c_\nu^{(a)})$. The energy decay of the solution to a diffusion equation is a well-known phenomenon. Here the problem comes from the fact that the diffusion coefficient $F_T^{\nu+1}(x)$ vanishes at the edge $x=1$. However, for $\nu > 1$, the decay rate of the diffusion coefficient ensures the convergence of the integral $X_0 = \int_0^1 F_T(x)^{-(\nu+1)/2}dx < \infty$. We have $X_0 \simeq 2.01$ for $\nu = 5/2$. We define the new spatial variable

$$X(x) = \int_x^1 F_T(x)^{-(\nu+1)/2}dx,$$

which is a one-to-one decaying function from [0,1] onto $[X_0, 0]$. We then define the new function $w(X,\tau) = \check{\xi}[x(X),\tau]$ which satisfies

$$\partial_\tau w = \partial_X^2 w + g(X)\partial_X w,$$

with the boundary conditions $w(\tau,0)=w(\tau,X_0)=0$. The function g is

$$g(X) = -\frac{\nu+1}{2}\partial_X(\ln\{F_T[x(X)]\}).$$

By differentiating the square $L^2(dx)$-norm of w, we get after a straightforward integration by part that

$$\partial_\tau \|w\|_{dx}^2 = -2\|\partial_X w\|_{dx}^2 - \int_0^{X_0} g'(X)w^2(X)dX.$$

Using the standard estimate $\|\partial_X w\|_{dx}^2 \geqslant (\pi^2/X_0^2)\|w\|_{dx}^2$ which holds true for any smooth function in $L^2(dx)$ with zero boundary conditions,[18] we obtain $\partial_\tau\|w\|_{dx}^2 \leqslant -\lambda^{(a)}\|w\|_{dx}^2$ with $\lambda^{(a)}=\pi^2/X_0^2+\min_{X\in[0,X_0]}[g'(X)/2]$. A numerical estimate yields $\min_{X\in[0,X_0]}[g'(X)] \simeq 1.18$ for $\nu=5/2$ so that $\lambda^{(a)} \simeq 3.03$. By integrating we get the exponential decay of the $L^2(dx)$-norm of w

$$\|w(\tau,\cdot)\|_{dx}^2 \leqslant \|w(0,\cdot)\|_{dx}^2 \exp(-2\lambda^{(a)}\tau).$$

This implies the exponential decay of the $L^2[F_T^{-(\nu+1/2)}(x)dx]$-norm of $\check{\xi}$ which in turn implies Eq. (22) with $c_\nu^{(a)}=A_\nu^{-1}\lambda^{(a)}$. □

Proof of Eq. (22) with $(\mu^{(b)},c_\nu^{(b)})$. An integration by part yields that

$$\partial_\tau\|\check{\xi}(\tau,\cdot)\|_{F_T^{-\nu-1}(x)dx}^2 = -2\|\partial_x\check{\xi}(\tau,\cdot)\|_{dx}^2.$$

Integrating this equation with respect to τ we get

$$\|\check{\xi}(\tau,\cdot)\|_{F_T^{-\nu-1}(x)dx} \leqslant e^{-2\lambda^{(b)}\tau}\|\check{\xi}(0,\cdot)\|_{F_T^{-\nu-1}(x)dx}$$

which implies (22) with $c_\nu^{(b)}=A_\nu^{-1}\lambda^{(b)}$ and $\lambda^{(b)}=\inf_\psi\|\partial_x\psi\|_{dx}$. The infimum is taken over all smooth functions ψ with $\psi(0)=\psi(1)=0$ and $\|\psi\|_{F_T^{-\nu-1}(x)dx}=1$. The operator $F_T^{\nu+1}(x)\partial_x^2$ is self-adjoint in the space $L^2(F_T^{-\nu-1}(x)dx)$. Using standard spectral theory tools we can compute the spectral representation of this operator. The first eigenvalues are $\lambda_1=-5.075$, $\lambda_2=-15.22$, $\lambda_3=-30.28$ for $\nu=5/2$. This spectral study demonstrates that $\lambda^{(b)}=-\lambda_1=5.075$.

[1] V. Lobatchev and R. Betti, Phys. Rev. Lett. **85**, 4522 (2000).
[2] R. Betti, M. Umansky, V. Lobatchev, V. N. Goncharov, and R. L. McCrory, Phys. Plasmas **8**, 5257 (2001).
[3] R. Betti, K. Anderson, V. N. Goncharov, R. L. McCrory, D. D. Meyerhofer, S. Skupsky, and R. P. J. Town, Phys. Plasmas **9**, 2277 (2002).
[4] M. C. Herrmann, M. Tabak, and J. D. Lindl, Nucl. Fusion **41**, 999 (2001).
[5] A. Kemp, J. Meyer-ter-Vehn, and S. Atzeni, Phys. Rev. Lett. **86**, 3336 (2001).
[6] S. Atzeni and M. Temporal, Phys. Rev. E **67**, 057401 (2003).
[7] J. D. Lindl, *Inertial Confinement Fusion* (Springer, New York, 1998).
[8] S. E. Bodner, Phys. Rev. Lett. **33**, 761 (1974).
[9] J. Sanz, Phys. Rev. Lett. **73**, 2700 (1994).
[10] V. N. Goncharov, R. L. Betti, R. L. McCrory, P. Sorotokin, and C. P. Verdon, Phys. Plasmas **3**, 1402 (1996).
[11] H. J. Kull, Phys. Fluids B **1**, 170 (1989).
[12] L. D. Landau and E. M. Lifshitz, *Fluid Mechanics* (Pergamon, New York, 1987), Chap. 89.
[13] Y. Saillard, in *Proceedings of the Inertial Fusion Sciences and Applications 2001*, edited by K. A. Tanaka, D. D. Meyerhofer, and J. Meyer-ter-Vehn (Elsevier, Paris, 2002), p. 192.
[14] R. Betti, V. N. Goncharov, R. L. McCrory, P. Sorotokin, and C. P. Verdon, Phys. Plasmas **3**, 2122 (1996).
[15] P.-A. Raviart and E. Godlewski, Laboratoire d'Analyse Numérique, Technical Report No. R03, 2000 (unpublished).
[16] V. N. Goncharov, Ph.D. thesis, University of Rochester, 1998.
[17] V. N. Goncharov, P. McKenty, S. Skupsky, R. Betti, R. L. McCrory, and C. Cherfils-Clérouin, Phys. Plasmas **7**, 5118 (2000).
[18] A. Friedman, *Partial Differential Equations* (Holt, Rinehart, and Winston, New York, 1969).